Journal of Applied and Computational Sciences in Mechanics. (25-40)

Ferdowsi University of Mashhad

Journal of Applied and Computational Sciences in Mechanics

Page Journal: mechanic-ferdowsi.um.ac.ir

Society of Manufacturing Engineering of Iran

Experimental Study to Obtain the Thermal Conductivity Coefficient of Concrete

Emad Prvazeh[1], Hadi Farzan[2], Mehran Ameri[3], Mohammad Shafiey Dehaj[4]

10.22067/jacsm.2025.90568.1295

The thermal performance of concrete plays a critical role in energy-efficient building design, particularly in structures integrating photovoltaic-integrated photovoltaic-thermal (PIPVT) systems, where enhanced heat transfer is essential for effective thermal energy recovery and photovoltaic temperature regulation. While most previous studies have focused on reducing the thermal conductivity of concrete for insulation purposes, limited research has addressed the development of thermally conductive concrete specifically tailored for solar-integrated applications. The novelty of this study lies in the experimental enhancement and quantification of concrete's thermal conductivity using iron shavings as a conductive additive, with results validated through a custom-designed measurement apparatus. Due to the limitations of conventional devices in accurately measuring the thermal properties of concrete, a dedicated experimental setup was developed and calibrated. The thermal conductivity of plain concrete was first determined, followed by mixtures incorporating approximately 2 weight percent(wt%) and 5.5wt% iron shavings,5%concrete concentrate, and a small amount of hemp fiber. The results showed increases in thermal conductivity of 53%,65%, and 30%, respectively, while the hemp fiber caused a slight reduction of 2%. A comparison between theoretical predictions and experimental measurements demonstrated approximately 85%agreement, confirming the reliability of the developed apparatus. These findings provide a material-level strategy for improving the heat transfer performance of building components integrated with PIPVT systems.

***Keywords*: Concrete, Thermal Conductivity, Iron Filings.**

I. Introduction

The thermal behavior of concrete has attracted significant research interest due to its dual impact on building energy performance and structural integrity. Among various thermal parameters, thermal conductivity(k) which quantifies the rate of heat transfer per unit temperature gradient plays a pivotal role in determining heat flow characteristics. Materials with low thermal conductivity are generally preferred for insulation applications, such as building envelopes or radiation shielding in nuclear facilities [1, 2]. In contrast, high-k materials are desirable for applications like heated floors and driveways with embedded heating systems [3]. Energy conservation has become essential amid growing populations and limited natural resources. Buildings account for approximately one-third of global energy consumption and 30% of greenhouse gas emissions in most countries [4, 5]. Since humans spend nearly 90% of their time indoors, energy efficiency and thermal comfort have gained increasing importance. Heating and cooling demands, as well as indoor comfort levels, are strongly influenced by the thermophysical properties of construction materials [6,7]. Thermal conductivity is also critical in controlling temperature-induced cracking in massive concrete elements, such as pavements, large foundations, and dams. For instance, Gui et al [8]. demonstrated that the thermal conductivity of pavement materials can exacerbate urban heat island effects by influencing surface temperature variations. The accumulation of mine tailings poses significant environmental challenges; however, incorporating these by-products as partial replacements for natural aggregates offers a sustainable alternative. In one study, the thermal conductivity of mortar samples with copper mine tailings (10–50%replacement of coarse aggregates) was evaluated using the transient line source method. Values increased consistently from 0.32W/m·K (reference) to 0.52W/m·K (50%substitution). ANOVA confirmed significant differences, with tailings proportion as the dominant factor. This enhancement is primarily attributed to the quartz-rich composition of the tailings, which improves heat conduction

* Manuscript received , Revised , Accepted. .

[1] PhD Candidate, Mechanical Engineering Department, Vali-e-Asr University of Rafsanjan, Rafsanjan, Iran.

[2] Associated Professor, Mechanical Engineering Department, Vali-e-Asr University of Rafsanjan, Rafsanjan, Iran.

[3] Professor, Mechanical Engineering Department, Shahid Bahonar University of Kerman University, Kerman, Iran.

[4] Corresponding Author. Associated Professor, Corresponding author. Mechanical Engineering Department, Vali-e-Asr University of Rafsanjan, Rafsanjan, Iran. **Email**: m.shafiey@vru.ac.ir.

compared to conventional aggregates [9]. Concrete, despite its widespread use, suffers from low tensile strength and brittleness. Partial cement replacement with pozzolans (e.g., fly ash), combined with steel fibers (0–1%) and iron filings (0–1%), can enhance mechanical properties. Tests on M25-grade concrete showed that steel fibers markedly improved compressive, tensile, and flexural strengths, while iron filings primarily boosted tensile and flexural strengths with limited impact on compression. Both additives slightly reduced workability, indicating their potential for property optimization [10]. Steel fibers available in forms such as straight, crimped, or hooked act as reinforcement, enhancing toughness and inhibiting crack propagation in steel fiber-reinforced concrete (SFRC). SFRC overcomes conventional concrete's brittleness and low tensile capacity, offering superior impact resistance, reduced spalling, and improved durability under freeze-thaw cycles and chemical exposure.

Environmental protection remains a key challenge in sustainable development, focusing on reduced energy use, conservation of raw materials, and waste minimization [11,12]. Recycling non-biodegradable wastes, such as fine iron filings, provides an effective solution for engineering applications [13]. Sargam et al. [14] found that supplementary cementitious materials (SCMs) and lightweight/recycled aggregates decrease thermal conductivity, whereas steel fibers above 0.25% increase it; polypropylene fibers showed no significant effect. Díaz and Hernandez [15] developed a custom device to measure thermal conductivity and resistance in concrete with recycled aggregates (including plastic waste and perlite), reporting substantial reductions in conductivity and improvements in resistance highlighting potential for energy-efficient buildings. Guo et al. [16] incorporated microencapsulated phase change materials (PCMs) into slag cement mortars for radiant floor heating, observing decreased density, strength, and conductivity with increasing PCM content (0–15%); a 1.97%PCM mixture offered the best balance.

Recent efforts to tailor concrete's thermal conductivity include graphite-modified recycled aggregates for enhanced conductivity without compromising strength [17], silicon carbide in pavements for improved thermal performance [18], natural/synthetic fibers for material-level effects [19], and graphite under high temperatures [20]. Despite extensive research, comprehensive studies on the effect of varying iron filings percentages on concrete thermal conductivity remain limited. Given iron's significantly higher thermal conductivity (~80 W/m·K) compared to plain concrete (~1–2 W/m·K), standard measurement devices may introduce errors. Thus, this study aims to quantify the increase in thermal conductivity with different iron filings contents to optimize efficiency in integrated solar pavements and thermal structures.

In recent years, numerous researchers have focused on solar energy, proposing diverse strategies to improve its efficiency [21]. These studies explore innovative approaches to enhance energy performance in solar systems and buildings from hybrid PVT-ST system development and climatic assessment to heat transfer enhancement via twisted tapes and advanced turbulators in collectors all aimed at boosting thermal and electrical efficiencies [22],[23]. Additionally, significant attention has been given to improving thermal comfort in buildings through optimized air distribution and phase change materials (PCMs) for energy savings. The findings demonstrate that integrating advanced technologies with optimized thermal design can markedly enhance energy efficiency, power output, and indoor thermal comfort [24], [25].

Although prior work has explored mineral/lightweight additives, limited attention has focused on thermally conductive concrete tailored for pavement-integrated photovoltaic-thermal (PIPVT) applications. In PIPVT systems, efficient heat transfer between photovoltaic modules and the supporting concrete is essential for temperature regulation and thermal energy recovery. The novelty of this research lies in experimentally evaluating iron filings as a conductive additive and assessing their quantitative impact at controlled weight fractions, bridging material-level modifications with system-level performance in integrated solar building technologies.

Functional additives such as metallic particles, graphite, or conductive fibers can markedly enhance concrete's thermal behavior. Iron shavings, in particular, along with graphite and certain fibers, facilitate efficient heat transfer in PIPVT systems critical for photovoltaic temperature control and energy recovery. These enhancements also benefit thermally active components like heated floors or industrial surfaces. By optimizing additive type and dosage, concrete can be engineered for both mechanical strength and superior thermal performance, supporting next-generation energy-efficient building materials.

His document is an example of the desired layout for a CKE Journal paper. It contains information regarding desktop publishing format, type sizes, and typefaces. Style rules are provided that explain how to handle equations, units, figures, tables, abbreviations, and acronyms. Sections are also devoted to the preparation of acknowledgments, references, and authors' biographies.

II. EXPERIMENTAL METHODS

A. *Thermal conductivity measurement box Set-up and preparation*

In one-dimensional conduction analysis, heat transfer is assumed to occur solely along one axis, with negligible contributions from other directions. This experiment was designed to achieve one-dimensional heat flow through forced convection induced by an electric heater [26]. Two identical glass boxes were constructed with internal dimensions of 24.5 cm (length) × 8.9 cm (width) × 7.3 cm (height). Each box was assembled and sealed using silicone adhesive, leaving one face (8.9 cm × 7.3 cm) open to accommodate the concrete specimen. After assembly, 3-mm-thick elastomeric insulation was applied around the edges of the concrete sample to thermally isolate the interior chamber. The inner surfaces of the box in contact with the specimen were fully lined with 3-mm self-adhesive elastomeric insulation to prevent air leakage. Once the concrete specimen is inserted, this configuration ensures no air exchange between the chamber interior and the external environment. Fig. 1 shows the fabricated boxes, the concrete sample placement area, and the insulation configuration, as further detailed in Fig. 2. As illustrated in Fig. 2, fiberglass insulation was applied to the external surfaces of both boxes. Fiberglass is recognized as one of the most effective thermal insulators for temperatures below 300 °C [27]. Its application minimizes heat losses through the outer surfaces, thereby enhancing the accuracy of heat transfer measurements and approximating ideal one-dimensional conduction conditions.

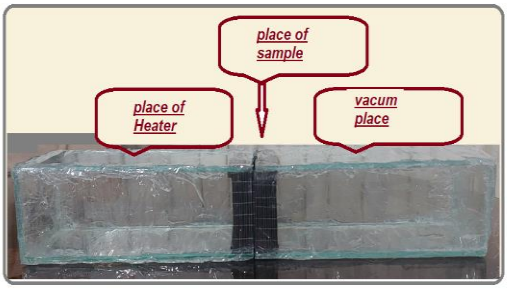

Fig. 1. Schematic of the box test

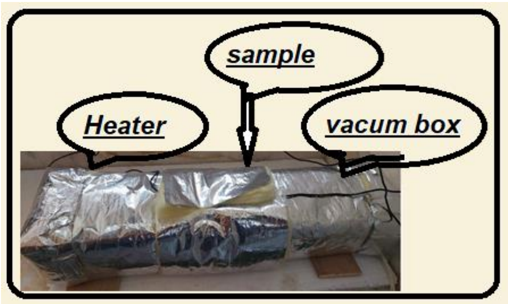

Fig. 2. Schematic of the box test

B. Sample Preparation

Concrete specimens were fabricated using molds constructed from rigid transparent plastic sheets. These molds were precisely cut to match the open face of the measurement box (89 × 73mm), with a thickness of approximately 21 mm to match the depth of the glass enclosure (Fig. 3a-b). The concrete mixtures were prepared based on the proportions listed in Table 1. Three different additives iron shavings, iron ore concentrate, and caulking thread were individually added to separate samples, each incorporated exclusively in one mix to evaluate their distinct thermal effects. The dimensions and specifications of each sample are provided in Table 2. After casting, the specimens remained in the molds at room temperature for 24 hours. Following demolding, they were exposed to direct sunlight for approximately 10 days to allow sufficient moisture evaporation, thus eliminating the need for conventional water curing. Prior to testing, the contact surfaces of the samples were carefully ground and smoothed using a grinder to ensure a tight fit within the measurement device and to prevent air leakage at the interface.

Table 1- Concrete mixing percentage

Sampel1	cement	Lightweight aggregate sand	water
percentage	18%	56%	26%

Table 2- Dimensions and types of additives incorporated into concrete specimens

No: sample	Size (L/W/H) (mm*mm*mm)	Additional material	Additional percent (weight of concrete)
1	90*74*18	-	-
2	86*68*21	iron filings	2%
3	87*67*22	iron filings	5.5%
4	90*74*18	hemp yarn	A few
5	86*69*20	Iron concentrate	5%

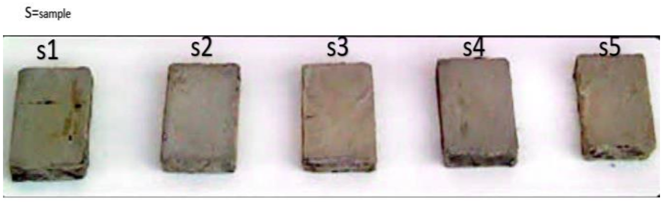

a

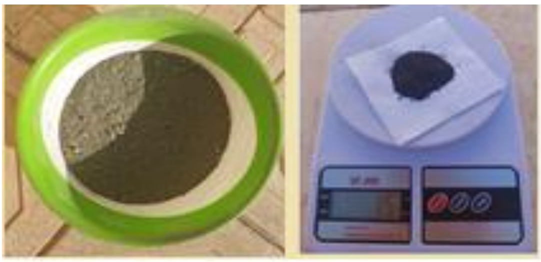

b

Fig. 3. a) Template making; b) Weighing; Mixture of materials

C. Concrete thermal conductivity measurement methods and strategies

In the present study, due to the unidirectional nature of heat transfer and the direct attachment of the heater to the concrete surface, only conduction is taken into account as the dominant heat transfer mechanism, while convective and radiative effects are assumed to be negligible. Based on the literature review, four common methods have been briefly outlined according to previous studies.

1) Steady state boxes method

The hot box method is a steady-state approach used to determine the thermal conductivity of concrete by evaluating the energy balance of the system. This method was developed in the laboratory for thermal and solar research at Claude Bernard University-Lyon I, France [28]. The experimental setup consists of a hot chamber and a cold chamber, with the specimen positioned between them. According to the second law of thermodynamics, heat flows from the hot side to the cold side. The thermal conductivity (k) is then calculated based on the temperature difference between the two chambers [29]. A schematic representation of the hot box method is illustrated in Fig. 4.

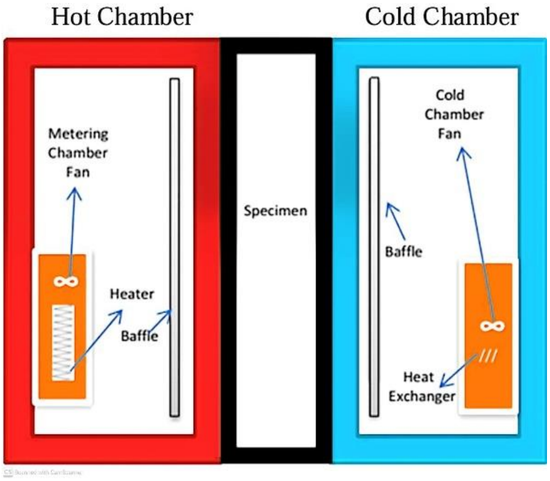

Fig. 4. Schematic of the box method

2) Steady state hot plate method

The guarded hot plate (GHP) method is widely used to evaluate the thermal conductivity of insulation materials. In this steady-state technique, the test specimen(s) are placed between a hot plate and a cold plate, while a steady heat flux is applied across the sample. The thermal conductivity is calculated based on the heat flow and the temperature difference between the surfaces of the specimen [30]. Gandage et al. [31] employed this method to measure the thermal conductivity of samples across five temperature levels, ranging from 30°C to 80°C. In a separate study, the cold plate was maintained at 18°C and the hot plate at 40°C [32]. A schematic diagram of the hot plate setup is shown in Fig. 5.

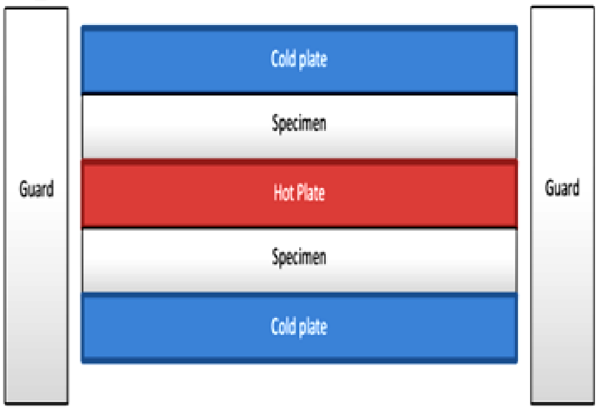

Fig. 5. Schematic of the hot plate method

3) Transient hot wire method (THW)

The transient hot wire method is a transient technique used to determine thermal conductivity by monitoring the temperature rise at a certain distance from a linear heat source embedded within the test material. The hot wire probe approach is based on the principles of the transient hot wire technique [33] and represents a modified version of the original method. Fig.6 illustrates the schematic concept of the hot wire method.

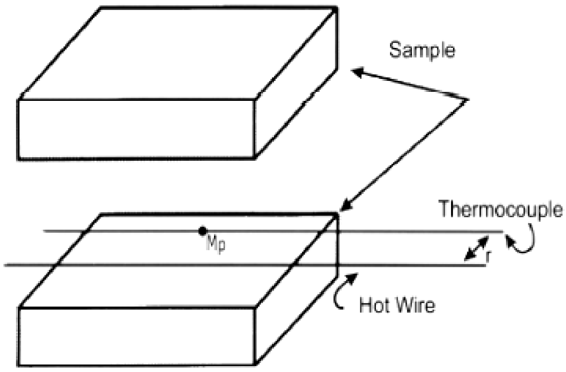

Fig. 6. Schematic of the hot wire method [34]

4) Transient plane source (TPS) method

This method determines thermal conductivity by analyzing the input power and the time-dependent temperature response of transient plane and transient line heat sources. The transient plane source (TPS) technique, in particular, is widely used to evaluate both in-plane and through-plane thermal conductivity of materials. In this approach, a flat spiral sensor acts simultaneously as a heat source and temperature sensor; its temperature rises as an electrical current passes through it (Fig. 7). By recording the temperature variations over time, the thermal properties (thermal conductivity, thermal diffusivity, and specific heat capacity) of the sample can be calculated using theoretical models based on the transient heat conduction equation.

Several studies have employed the TPS method to investigate the effects of additives on concrete thermal conductivity. For instance, the addition of wood shavings to sand-based concretes has been shown to reduce thermal conductivity. Additionally, the influence of moisture content on the thermal conductivity of autoclaved aerated concrete (AAC) and the impact of different aggregate types on the k-value of concrete under relative humidity conditions ranging from 10% to 30% have been explored [35–38].

Fig. 7. Transient plane source method [39]

The thermal conductivity of concrete samples was evaluated using a modified guarded hot plate method, a steady-state technique well-established for its precision in testing construction materials (ASTM C177; ISO 8302). In this experimental arrangement, one surface of the concrete specimen was exposed to a controlled heat source, while the opposite surface was fitted with a high-accuracy temperature sensor to monitor the temperature gradient. Both sides of the specimen were enclosed within an insulated chamber, which minimizes lateral heat losses and ensures that heat transfer occurs predominantly in one dimension. This setup allows nearly the entire heat flux to pass through the sample, providing measurements that reliably reflect the intrinsic thermal properties of the concrete. The temperature difference across the specimen and the applied heat flux were recorded simultaneously, enabling calculation of thermal conductivity under steady-state conditions. By effectively reducing convective and radiative losses to the environment, this method generates highly dependable data. The collected results can also support advanced thermal modeling for concrete pavements, foundations, and other structural components, allowing accurate predictions of heat transfer behavior in both laboratory and practical engineering applications.

D. Experimental Set-up and Methodology

1) Materials & Methodology

To accurately evaluate the thermal conductivity of concrete, a custom-designed experimental setup was developed and operated under fully controlled conditions. Three types of rectangular concrete specimens were prepared: (i) plain concrete, (ii) concrete containing 2wt% iron shavings, and (iii) concrete containing 5.5wt% iron shavings. Selected mixtures also incorporated 5wt% concrete concentrate and a small proportion of hemp fiber to assess their combined influence on thermal performance. All specimens were cured under standard laboratory conditions for 28 days prior to testing. Thermal conductivity measurements were conducted at a controlled ambient temperature of 25 ± 2 °C and relative humidity of 10 ± 5%. The experimental apparatus employed a steady-state heat flow configuration, with multiple thermocouples strategically embedded at precise locations within the specimens to accurately capture the temperature gradients. Each test was performed in triplicate to ensure data reproducibility and reliability. The experimental procedure strictly adhered to standard guidelines for steady-state thermal conductivity measurements of solid materials.

Environmental heat losses were carefully minimized through insulation and subsequently corrected in the data analysis. Detailed information on the apparatus design, calibration procedure, and measurement protocols is provided to ensure transparency and facilitate reproducibility by other researchers. This methodology enables a precise assessment of how different conductive additives such as iron shavings and fibers affect the thermal performance of concrete, offering valuable insights for applications in energy-efficient building systems and pavement-integrated photovoltaic-thermal (PIPVT) structures.

2) auxiliary components

The overall experimental setup is presented schematically in Fig. 2. Due to space limitations within the apparatus, a yellow incandescent bulb with a flat front and a rated power of 40 W was used as the heat source. The bulb was mounted directly onto the surface of the concrete specimen to ensure efficient conductive. According to both manufacturer data and literature, incandescent bulbs typically convert around 90-95% of electrical energy into heat and only about 5-10% into visible light, making them suitable for thermal studies.

To reduce undesired heat losses, the bulb was surrounded by fiberglass insulation. Surface temperatures of the concrete were measured using two digital thermometers. Additionally, a multimeter was connected to the circuit to record voltage and current, enabling precise calculation of the power supplied to the heating element. Electrical power was transmitted via flexible copper wires with a cross-sectional area of 1.5 mm^2, providing low resistance and safe operation. Furthermore, a thermal imaging camera (FLIR E60) was employed to capture infrared images of both the surface and cross-section of the concrete for detailed temperature mapping and analysis.

3) Set-up sensors

To ensure accurate evaluation of the thermal behavior, heat transfer characteristics, and thermal conductivity of the concrete specimens, precise temperature measurements on both surfaces were essential. For this purpose, digital thermometers (model TPM10) were employed to record the temperatures at the hot and cold surfaces of the concrete specimen. The exact placement and positioning of the temperature sensors are illustrated in Fig. 8. All recorded temperature data were transmitted to a computer via a data acquisition system for real-time monitoring, logging, and subsequent analysis, including the determination of the temperature gradient (ΔT) required for thermal conductivity calculations.

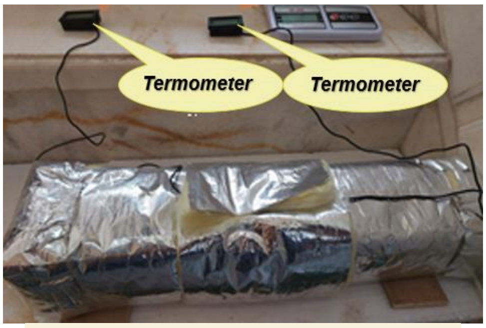

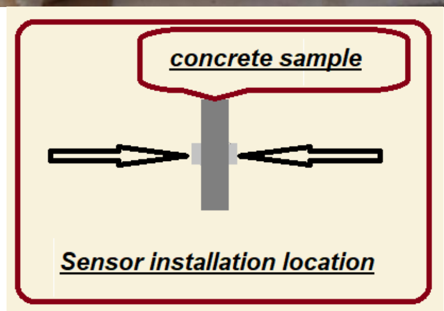

Fig. 8. The final device under test

E. Test method

All experiments in this study were conducted at the Energy Laboratory of Vali-e-Asr University of Rafsanjan, Iran (30°24′N, 55°55′E), with an average city elevation of approximately 1469 m above sea level. The experimental measurements were carried out between 8:30 a.m and 3:30 p.m under field conditions during the summer of 2025. Days with extreme environmental conditions, such as high winds, cloudy skies, or dusty atmospheres, were excluded from the analysis. For each experiment, the concrete specimen was positioned at the designated location, and the heater was securely attached to its surface. Two temperature sensors were installed on opposite sides of the specimen, with the recorded values transmitted to a digital temperature display unit via connecting wires. Initially, the heater operated for 15–20 minutes to ensure uniform heating and achieve thermal equilibrium. Once steady-state conditions were reached, the temperatures of both surfaces were measured continuously for approximately 5minutes. After each test, the specimen was replaced, and the procedure was repeated for all samples. All data were logged and subsequently transferred to a computer for thermal conductivity calculations and further analysis. In a separate experiment, the concrete specimens were exposed to direct sunlight for six hours, during which infrared thermal images were captured to map surface temperatures. Specific points on the thermal images were selected, and the corresponding temperatures were extracted and recorded for further thermal performance evaluation. Additionally, cross-sectional thermal images were obtained from three different concrete specimens. For each cross-section, three measurement points (top, middle, and bottom) were identified, and the temperatures at these points were recorded and stored in a computer system for detailed thermal analysis.

III. THEORY STATEMENT AND FORMULATION

There are two methods for supplying heat to the wall surface, each requiring a specific equation for calculating the thermal conductivity. These methods and their corresponding formulations are described in detail below. In this experiment, the first method based on electrical power input was employed. By equating the electrical power with the heat conduction rate from Fourier’s law, the thermal conductivity of the concrete sample was determined.

To simulate a heat source, a certain amount of energy must be given to the object, which is provided by the heater. According to Eq.1, and using a multimeter, the heater power, voltage, and current are obtained, respectively. [40]

$$Q = VI \tag{1}$$

It is worth noting that a container of boiling water can be used to calculate the heat transfer to the wall and, ultimately, the amount of heat transferred can be calculated using below equation:

$$Q = hA(T2 - T1) \tag{2}$$

Materials with low to moderate thermal conductivity, such as mineral wool (0.03–0.04 W/m·K), cellulose insulation (0.04–0.05 W/m·K), cork (0.04–0.05 W/m·K), expanded polystyrene (EPS, 0.03–0.04 W/m·K), polyurethane (0.02–0.03 W/m·K), wood (0.14 W/m·K), and ceramic tiles (1.10 W/m·K) are effective in reducing energy consumption in buildings [41, 42]. The rate of heat transfer per unit area across a surface can be calculated using Fourier’s law [43]:

$$q = -k\,.\,\nabla T = -k(i\frac{\partial T}{\partial x} + j\frac{\partial T}{\partial y} + k\frac{\partial T}{\partial z}) \tag{3}$$

When the heat flow is only in one direction (Fig. 9), the above equation is simplified to:

$$q = -k(\frac{\partial T}{\partial x}) \tag{4}$$

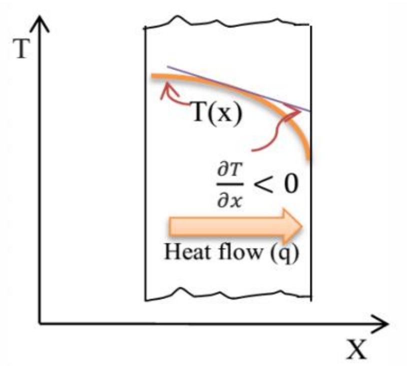

Fig. 9. Schematic of one-dimensional heat transfer by conduction [44]

The heat flow rate calculates by below relation:

$$Q = qA \tag{5}$$

Therefore, Q is:

$$Q = -kA(\frac{\partial T}{\partial x}) \tag{6}$$

Concrete is a common material all over the world and more than ten billion tons of concrete are produced every year [45].

IV. EXPERIMENTAL UNCERTAINTY ANALYSIS

In any experimental study, the reliability of the results largely depends on the precision of the measurements and a comprehensive evaluation of their associated uncertainties. The accuracy of an instrument indicates how closely a measured value aligns with the true or accepted reference value. While accuracy primarily reflects systematic errors, uncertainty analysis accounts for both systematic and random errors to quantify the overall doubt in a measurement. In this research, uncertainties were estimated following the approach proposed by Kline and McClintock [46]. The method is expressed in Eq. (7):

$$w_R = \left[\sum_{i=1}^{n} \left(\frac{\partial R}{\partial x_i} w_{x_i} \right)^2 \right]^{1/2} \tag{7}$$

TABLE 3
Table 3- The uncertainty and accuracy of main factors

parameter	Range	Accuracy	Uncertainty
Thermometer	0-100	0.5	0.5%
Heater	40	1	2.5%
Weighing machine	0-1	0.1	0.01%
Multimeter	0-400	0.1	0.025%
Fourier's law	N. A	N. A	2.5%

where W_R is the uncertainty in the result (dependent parameter), W_{xi} are the uncertainties in the independent variables, $\frac{\partial R}{\partial x_i}$ are the sensitivity coefficients (partial derivatives), and n denotes the number of independent variables. Table 3 summarizes the accuracy and uncertainty associated with the key measured and calculated parameters. The overall experimental uncertainty was calculated using the Kline and McClintock error propagation method. Considering the uncertainties of the thermometer (±0.5%), heater (±2.5%), weighing machine (±0.01%), multimeter (±0.025%), and Fourier's law-based thermal conductivity calculations (±2.5%), the combined uncertainty of the experimental measurements was estimated to be approximately 3.57%. The dominant sources of uncertainty were associated with the weighing system and the Fourier's law-based calculations, while the contribution of the multimeter was negligible.

V. Validation of Thermal Conductivity Results

The measured density of the concrete specimen was 1780 kg/m³, which lies within the transition range between semi-lightweight and normal-weight concrete. Previous studies have shown that concrete in this density range typically exhibits thermal conductivity values between1.6and1.9W/m·K[47–48]. To quantify the agreement between the experimental results and theoretical data, the relative agreement percentage was calculatedas. Where k_{exp}=1.9 w/m.k and k_{ref}=1.6.

$$\text{Agreement (\%)} = (1-\frac{|k_{exp}-k_{ref}|}{k_{ref}})*100 \quad (8)$$

Based on this calculation, the agreement is approximately 85%, indicating good consistency with theoretical expectations. Minor discrepancies may be attributed to moisture content and aggregate properties.

VI. Results and discussion

Heat transfer is a vector quantity that can simultaneously occur via conduction, convection, and radiation. In solid materials, conduction arises from the combined effects of molecular vibrations in the crystal lattice and energy transport by free electrons. This mechanism is crucial for assessing the thermal performance of building materials and structural components. The thermal conductivity (K-value) represents a key material property that quantifies a material's capacity to conduct heat. Since the thermal conductivity of construction materials varies depending on their application—such as in floors, walls, or other structural elements—this property directly influences building energy consumption and overall energy efficiency. Accordingly, precise and reliable measurement of thermal conductivity is essential for evaluating the thermal performance of buildings and predicting the practical thermal behavior of materials [49–51].

A. In the present study, five slabs made from different materials were fabricated, with the specifications of each slab summarized in Table 2.

The experimental procedure involved applying heat flux through each slab over a defined period while precisely measuring the temperatures on both opposing surfaces. Using the obtained temperature data, the heat transfer coefficient for each slab was calculated based on Fourier's law. These calculations enabled a direct comparison of the thermal performance of the different materials and provided insight into the actual behavior of each material under realistic heat transfer conditions. The results of these experiments are presented in Table 4, and the analysis indicates that variations in the thermal conductivity of the materials significantly influence the thermal performance of the slabs. This information is crucial for optimized building design, appropriate material selection, and reducing energy consumption. Moreover, the provision of accurate thermal conductivity data serves as a basis for further studies and the development of numerical models to predict the thermal behavior of building components.

Table 4- Results of tests

No: sample	K (w/m. ºk)	C_p (j/g . ºc)
1	1.9	0.71
2	2.92	0.70
3	3.15	0.69
4	1.87	0.72
5	2.47	0.70

As shown, the variations in C_p among the samples are relatively small (0.69–0.72). The slight decrease in C_p for the iron-containing samples is consistent with the lower specific heat capacity of iron compared to concrete. In contrast, the sample containing hemp fibers exhibits a slightly higher C_p, which can be attributed to the higher thermal capacity and insulating properties of the fibers. These results indicate that the addition of small amounts of iron or hemp does not significantly alter the heat storage capacity of the concrete, although the observed variations logically reflect the type and proportion of the additives. This discussion helps to better understand the thermal behavior of modified concrete.

The 85% agreement between the data extracted from the experimental results and the data obtained from the theoretical relationships indicates the high accuracy of the experiment and study.

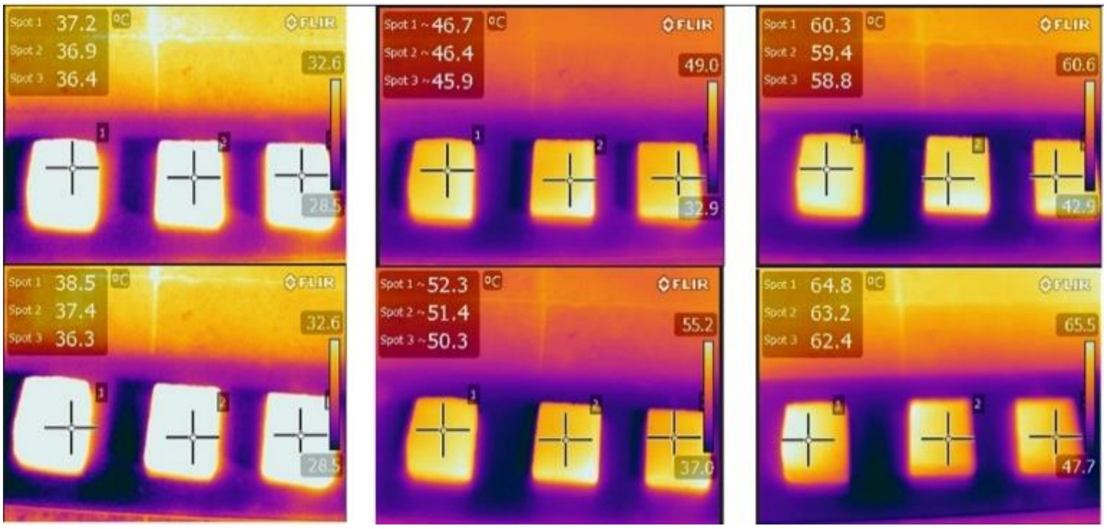

Fig. 10. Temperature changes of concrete surface

Table 5- Comparison of additives used in the study

No: sample	Main function	Effect on thermal conductivity	Other effects
1		baseline	
2	Increase heat transfer	+53% increase	Slight density increase
3	Enhance thermal pathway formation	+65% increase	Improved thermal network formation
4	Increased porosity and air entrapment	-2% decrease	Improved crack control &ductility
5	Increased solid conductive phase fraction	+30% increase	Improved crack control ductility

B. Experimental Procedure and Surface Temperature Analysis of Concrete Slabs under Sunlight

In this study, three concrete slabs, whose specifications are provided in Table 6, were exposed to direct sunlight from 6:00am to 3:00pm to evaluate the effect of metallic additives on the surface temperature of concrete. Thermal imaging of the slabs was performed at one-hour intervals, with the first image captured at approximately 8:00 am. All thermal images were recorded using a FLIR E60 infrared camera, ensuring accurate and high-resolution data for analyzing surface temperature distribution. The captured images are presented in Fig. 10.

Table 6- Sample of test (samples for the sunlight exposure test)

No: sample	No: spot	Additional material	Additional percent (weight of concrete)
1	1	-	-
2	2	iron filings	2%
3	3	iron filings	5.5%

Analysis of the thermal images indicated that the slab containing a higher proportion of iron filings consistently exhibited a lower surface temperature compared to the other slabs. This observation aligns with fundamental physical principles, as iron filings possess a higher thermal conductivity. The increased amount of iron filings enhances the overall thermal conductivity of the concrete, allowing absorbed solar energy to be more effectively distributed throughout the slab. Consequently, the surface temperature of the iron-rich slab remains lower than that of the other specimens, reflecting its improved heat dissipation capability provided by the metallic additives. These results demonstrate that the incorporation of iron filings into concrete not only modifies the thermal properties of the material but also serves as an effective strategy for improving surface thermal performance under direct sunlight. Such modifications can have significant practical implications for reducing surface heat effects, optimizing energy management in buildings, and designing sustainable structures in regions with high solar radiation. Furthermore, the collected thermal data provide a valuable foundation for numerical modeling and advanced simulation studies, enabling more accurate prediction of the thermal behavior of concrete materials under realistic environmental conditions. This information can guide the selection of construction materials and the design of structures, particularly in applications where thermal performance is of critical importance.

Table 7- Surface temperatures of concrete slabs

t	**T1 (C°)**	**T2 (C°)**	**T3 (C°)**	**R1**	**R2**
8:00	37.2	36.9	36.4	0.8	2.1
9:00	38.5	37.4	36.3	2.9	5.7
10:30	46.7	46.4	45.9	0.6	1.7
12:00	52.3	51.4	50.3	1.7	3.8
13:15	60.3	59.4	58.8	1.5	2.5
14:45	64.8	63.2	62.4	2.5	3.7

$$R = \frac{T_1 - T_2}{T_1} * 100 \quad (9)$$

when; R_1 is Reduction vs Sample1(%) Sample2; R_2 is Reduction vs Sample1(%); T_1 is Temperature of surface (C^o)-sample1; T_2 is Temperature of surface (C^o)- sample2; T_3 is Temperature of surface (C^o)- sample3 and t is Time (H h: mm).

The experiment started at 08:00 am, and surface temperature measurements were taken at different time intervals, as summarized in Table 7. At the beginning of the experiment, the surface temperatures of all specimens were approximately similar. The initial surface temperature of the plain concrete slab (without any additives) was 37.2 °C. The slab containing 2wt% iron filings showed a surface temperature of 36.9°C, while the slab with 5.5wt% iron filings exhibited a lower surface temperature of 36.4°C. The observed temperature reduction varies at different measurement times. This variation can be attributed to the progressive accumulation of thermal energy in the slabs and the influence of environmental conditions throughout the day. Slabs containing iron filings consistently exhibited lower surface temperatures compared to the plain concrete slab at all measurement times. This is primarily due to the higher thermal conductivity of metallic additives, which create additional conductive pathways, allowing absorbed solar energy to be more effectively distributed throughout the slab and reducing surface temperature. On average, each 1wt% increase in iron filings results in approximately a 0.5% decrease in the surface temperature of the concrete. In addition, the gradual increase in surface temperature over time reflects the storage of thermal energy within the concrete, as the material absorbs heat and gradually transfers it throughout the slab. Table 7, summarizes the surface temperatures of the concrete slabs at different times and the corresponding reduction in surface temperature relative to the plain concrete slab. Slabs with metallic additives displayed more uniform temperature distributions and lower surface temperature peaks, confirming the enhanced heat dissipation capability provided by the iron filings. These findings provide a quantitative basis for optimizing the use of metallic additives to improve surface thermal performance in building materials and serve as a foundation for numerical modeling and advanced simulation studies.

C. Experimental Procedure and Surface Temperature Analysis of Concrete Slabs under Sunlight (The concrete specimen containing the highest proportion of iron filings was considered as the reference slab)

Thermal Response Analysis of Concrete Specimens with Various Additives under Solar Irradiation In this experimental investigation, three concrete specimens, whose detailed specifications are provided in Table 7, were exposed to uniform solar irradiation to evaluate the influence of different additives on surface temperature and overall thermal behavior. Among the tested samples, the concrete specimen containing the highest proportion of iron filings was designated as the reference slab, providing a baseline for comparative analysis. The experiment commenced at 6:00 am, and thermal imaging was performed at approximately one-hour intervals, with the first image captured at 8:00 am using a FLIR E60 infrared thermographic camera. This high-resolution imaging method allowed for precise measurement and visualization of the temperature distribution across the slab surfaces over time. The thermal images are presented in Fig. 11.

Table 8- Sample of test (samples for the sunlight exposure test)

: sample	No: spot	Additional material	Additional percent (weight of concrete)
1	1	iron filings	5.5%
2	2	hemp yarn	A few
3	3	Iron concentrate	5%

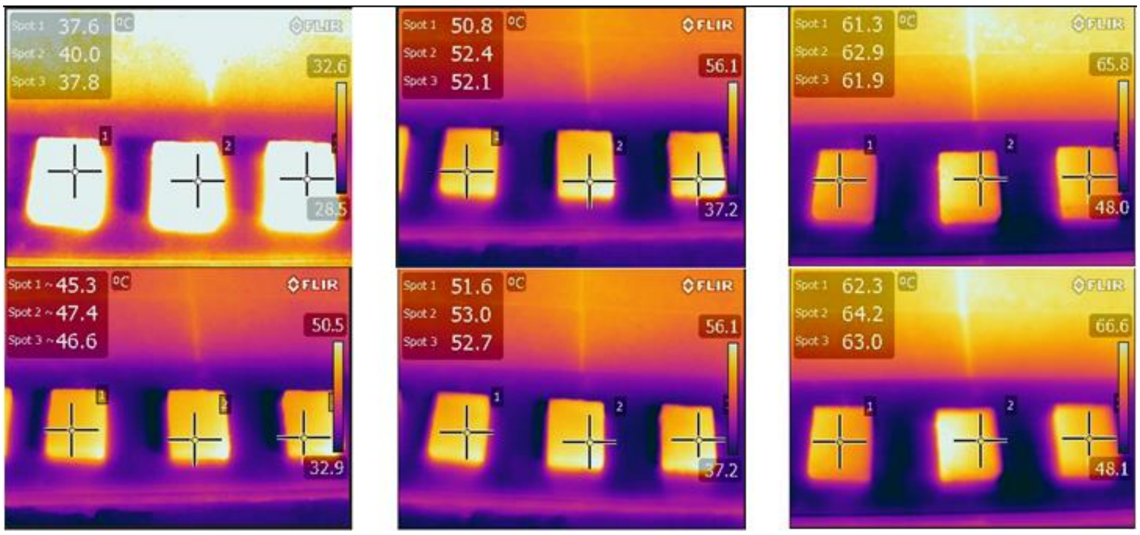

Fig. 11. Temperature changes of concrete surface Containing Iron Filings with Other Additives

To assess the effect of different additives, two additional specimens were prepared: one containing iron concentrate and another reinforced with hemp fibers. The main objective was to examine how these additives modify the surface temperature distribution and affect the heat transfer characteristics of the concrete under identical environmental conditions. Quantitative and qualitative analysis of the thermographic images revealed that the reference specimen consistently exhibited lower surface temperatures compared to the other two specimens. This behavior is consistent with the higher thermal conductivity of the iron filings concrete, which enables more efficient heat transfer from the surface into the interior of the material. In contrast, the slabs containing iron concentrate and hemp fibers showed relatively higher surface temperatures, indicating slower heat dissipation and altered thermal transport properties due to the differing nature, composition, and spatial distribution of the additives. The results highlight the critical role of additive type, content, and distribution in regulating the thermal performance of concrete. Incorporating high-conductivity materials, such as iron filings, can significantly improve heat transfer, thereby reducing surface heat accumulation and mitigating potential thermal stresses. These findings have practical implications for the design and optimization of energy-efficient building envelopes, solar-exposed concrete surfaces, and sustainable structural applications in regions with high solar radiation. Furthermore, the collected thermal data provide a robust foundation for numerical modeling and advanced simulation studies, allowing for more accurate prediction of concrete thermal behavior under realistic outdoor conditions. Such simulations can assist engineers and researchers in material selection, structural design, and performance optimization, particularly for applications where thermal management is critical. Overall, this study demonstrates that careful selection and proportioning of additives can substantially enhance the thermal performance of concrete, offering opportunities for improved energy efficiency, durability, and sustainable construction practices in environments exposed to intense solar radiation. These findings contribute to a better understanding of how additive-enhanced concrete can be tailored to meet specific thermal performance criteria in modern building and infrastructure projects.

The experiment was conducted on concrete slabs with different additives: one containing 5.5wt% iron filings, another containing a small amount of hemp fiber, and a third containing 5wt% iron concentrate. Surface temperature measurements were taken at different time intervals throughout the experiment. At the beginning of the experiment, the surface temperatures of all specimens were relatively similar. Over time, all slabs exhibited a gradual increase in surface temperature due to the accumulation of thermal energy. Notably, the concrete containing hemp fiber consistently showed higher surface temperatures compared to the slabs with metallic additives, while the slab with 5.5wt% iron filings exhibited the lowest surface temperature throughout most measurement times. The slab with iron concentrate displayed intermediate behavior, with surface temperatures lower than the hemp-containing slab but slightly higher than the iron filings slab. The lower surface temperature of the slabs containing metallic additives is primarily attributed to their higher thermal conductivity, which facilitates more efficient heat dissipation throughout the concrete. In contrast, the fibrous additive limits heat transfer within the slab, resulting in higher surface temperatures. The gradual increase in surface temperature over time for all slabs reflects the storage of thermal energy within the concrete, as heat is absorbed and gradually transferred throughout the material. These observations confirm that the type and amount of additive have a significant influence on the thermal performance of concrete. Metallic additives enhance heat dissipation and lower surface temperatures, while fibrous additives with low thermal conductivity tend to retain heat at the surface. These findings provide a solid foundation for optimizing additive selection to improve the thermal performance of concrete in building applications and can guide numerical modeling and advanced simulation studies.

D.Temperature Distribution in the Minimum Cross-Section of Three Concrete Specimens

Table 9- Sample of test (samples for the cross-section temperature test)

No: sample	Additional material	Additional percent (weight of concrete)
1	-	-
2	iron filings	2%
3	iron filings	5.5%

Infrared thermal imaging was performed on the cross-sections of three concrete specimens, the detailed compositions of which are provided in Table 8. For each specimen, temperatures were recorded at three predefined points located at the bottom, center, and top of the cross-section. The collected temperature data were then plotted on a comparative graph to assess the thermal distribution patterns as shown in Fig.12. Based on the results, the concrete sample incorporating 5.5wt.% iron filings exhibited the most uniform temperature distribution. This behavior is primarily attributed to the relatively high thermal conductivity of iron particles, which facilitates more effective heat transfer within the matrix. The observed uniformity also supports the accuracy and consistency of the experimental setup and measurement process.

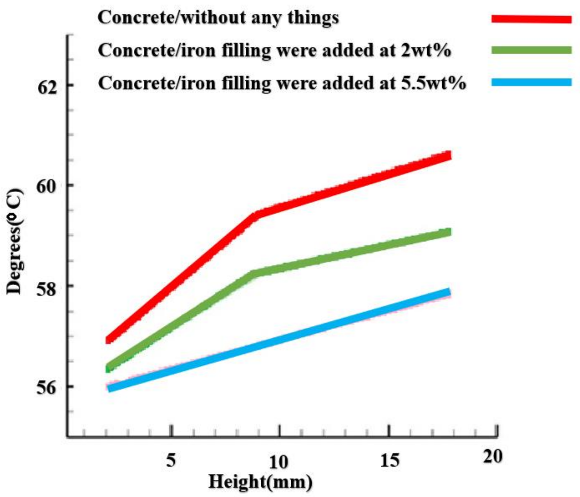

Fig. 12. Temperature distribution across the cross-section of three concrete samples (2mm/9mm/18mm) (Lines are drawn as visual guides only)

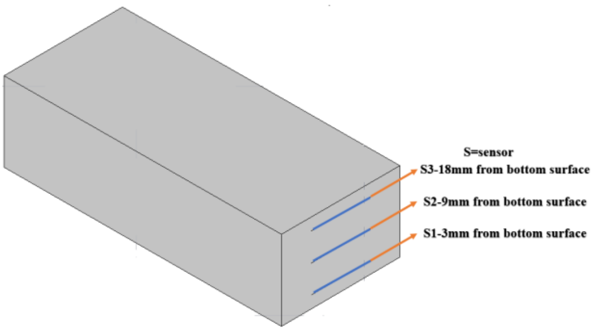

Fig. 13. Placement of temperature sensors within the concrete slab. (S1, S2, and S3 are positioned at 3 mm, 9 mm, and 18 mm from the bottom surface, respectively) (To capture the thermal gradient across the slab thickness)

To evaluate the temperature distribution across the specimen thickness, thermal measurements were performed at three discrete depths (2 mm, 9 mm, and 18 mm) from the cross-sectional surface using infrared thermography. These points represent localized temperature values along the primary heat transfer direction. Considering that heat transfer within the concrete specimens is predominantly governed by one-dimensional conduction through the thickness, and that internal heat generation during the experiment was negligible, the thermal behavior of the system can be described by Fourier's law of heat conduction. Under quasi-steady-state conditions and assuming homogeneous effective thermal conductivity at the macroscopic scale, the governing heat conduction equation simplifies to:

To evaluate the temperature distribution across the specimen thickness, thermal measurements were performed at three discrete depths (2 mm, 9 mm, and 18 mm) from the cross-sectional surface using infrared thermography. These points represent localized temperature values along the primary heat transfer direction. Considering that heat transfer within the concrete specimens is predominantly governed by one-dimensional conduction through the thickness, and that internal heat generation during the experiment was negligible, the thermal behavior of the system can be described by Fourier's law of heat conduction. Under quasi-steady-state conditions and assuming homogeneous effective thermal conductivity at the macroscopic scale, the governing heat conduction equation simplifies to:

$$\frac{d^2T}{dx^2}=0 \tag{10}$$

The analytical solution of this equation yields a linear temperature distribution across the thickness:

$$T(x) = Ax + B \tag{11}$$

Accordingly, the connection of the measured data points in the figure is intended to represent the physically expected linear temperature gradient under steady conductive conditions, rather than arbitrary interpolation between discrete measurements. Given the limited specimen thickness and the stabilized thermal state during data acquisition, the linear approximation of the temperature profile is thermodynamically justified.

Experimental observations demonstrated that incorporating iron filings into the concrete matrix significantly reduced the slope of the surface temperature variation curve along the specimen's height compared to conventional concrete. This effect is primarily attributed to the enhanced effective thermal conductivity of the composite, whereby the dispersed metallic particles establish highly efficient conductive pathways that facilitate faster and more uniform heat distribution throughout the specimen. Consequently, localized temperature gradients are diminished, and the rate of surface temperature change is substantially lowered. Such thermophysical behavior offers considerable advantages in applications requiring efficient heat dissipation and mitigation of thermal hotspots, particularly in photovoltaic–thermal concrete systems where thermal management plays a critical role in enhancing overall energy conversion efficiency. thermal imaging results confirmed that the addition of iron filings led to a reduction in the concrete surface temperature compared to plain concrete. This phenomenon supports the increased effective thermal conductivity resulting from the metallic particles that form efficient heat conduction pathways, leading to decreased localized temperature gradients and reduced rates of surface temperature variation.

VII. Conclusion

Based on the finding in this research:

A. *Enhancement of thermal conductivity*

Incorporating iron filings into the concrete matrix resulted in a measurable improvement in thermal conductivity across all investigated replacement levels. Prior experimental findings also reported that the addition of iron filings slightly increased the thermal conductivity of concrete, owing to enhanced thermal pathways and increased density of the composite.

B. *Optimal dosage identification*

The optimal iron filings content was determined to be 5.5wt.% of cement, yielding the maximum improvement in thermal conductivity relative to the control sample. Although direct matches for this exact percentage were not found in existing literature, comparable studies such as those by Kanibou et al. [52] demonstrated that adding iron powder (5–25% by weight as sand replacement) significantly enhanced thermophysical properties like thermal conductivity.

C. *Performance decline at higher contents*

While higher dosages still achieved thermal conductivity superior to the reference mix, slight declines in performance were observed beyond the optimal level. This curvilinear trend—where excessive additive content may introduce microstructural heterogeneities and diminish efficiency mirrors the observations in concrete reinforced with iron waste and fibers, where benefit peaks at moderate contents.

D. *Potential for specialized applications*

The data indicate that the optimized mix designs are promising for specialized construction systems such as integrated thermal–photovoltaic pavements (PIPVT), which combine thermal energy storage with electricity generation. PIPVT technology has been proposed as an innovative approach to exploit expansive urban infrastructures like pavements for dual energy production and surface cooling.

E. Effect of moderate additive content

A modest increase of 3.5wt.% iron filings was associated with approximately 15% enhancement in thermal conductivity. This underscores that even small proportions of conductive material can significantly improve heat transfer without severely compromising structural integrity a principle also supported by studies showing that moderate replacements boost mechanical properties while higher contents may introduce weaknesses.

F. Investigating and announcing the overall result of whether the heat transfer coefficient of concrete increases or decreases due to additives

The experimental results show that metallic additives markedly improve concrete's thermal conductivity compared to the control sample. Adding 2wt% iron shavings increased thermal conductivity by ≈53%, while 5.5wt% yielded ≈65%. This enhancement results from iron's high conductivity and formation of conductive pathways; however, gains appear non-linear at higher contents due to possible agglomeration. Iron concentrate produced a moderate ≈30% increase, likely due to finer particle size, uniform distribution, and weaker conductive bridging compared to irregular shavings. In contrast, 2wt% hemp fibers caused a slight reduction, consistent with their low intrinsic conductivity and induced microvoids/porosity that increase thermal resistance. These findings highlight metallic additives especially iron shavings as effective for enhancing heat transfer in concrete, with strong potential for PVT-integrated building systems where better heat extraction from PV modules improves temperature regulation, electrical efficiency, and energy yield. Optimizing additive type and dosage offers a viable strategy for advanced thermally conductive structural materials.

Table 10- Final test results on whether the heat transfer coefficient is increasing or decreasing

No concrete sample	Additional material	Additional percent (weight of concrete)	Effect on heat transfer coefficient (percentage of increase or decrease)
1	Without any thing	-	-
2	iron filings	2%	53% increase
3	iron filings	5.5%	65% increase
4	hemp yarn	A few	2% decrease
5	Iron concentrate	5%	30% increase

G. Thermal characterization of iron-modified Concrete for PIPVT applications

The primary contribution of this study is the experimental validation of a thermally enhanced concrete mixture suitable for PIPVT-integrated structures. The incorporation of small weight fractions of iron filings significantly increases thermal conductivity, facilitating improved heat transfer within structural elements. This material-level enhancement can contribute to more efficient thermal energy extraction, reduced photovoltaic operating temperatures, and improved overall performance of PIPVT systems. The results provide a practical and scalable approach for designing energy-active structural materials in next-generation solar-integrated buildings.

NOMENCLATURE

Q Heating Power (W)
V Voltage across the heater (V)
I Current through the heater (A)
h Convective heat transfer coefficient ($W/m^2.^oc$)
A Concrete surface(M^2)
T Temperature(^oC)
K Thermal conductivity of concrete ($W/m.^oc$)
L Length of concrete (mm)
W Width of concrete (mm)
H Height (or thickness) of concrete (mm)

REFERENCES

[1] D. T. C. P. Campbell‐Allen and C. P. Thorne, "The thermal conductivity of concrete," *Magazine of Concrete Research*, vol. 15, no. 43, pp. 39–48, 1963. https://doi.org/10.1680/macr.1963.15.43.39

[2] M. I. Khan, "Factors affecting the thermal properties of concrete and applicability of its prediction models," *Building and Environment*, vol. 37, no. 6, pp. 607–614, 2002. https://doi.org/10.1016/S0360-1323(01)00061-0

[3] A. L. Marshall, "The thermal properties of concrete," *Building Science*, vol. 7, no. 3, pp. 167–174, 1972. https://doi.org/10.1016/0007-3628(72)90022-9

[4] D. Zhang, Z. Li, J. Zhou, and K. Wu, "Development of thermal energy storage concrete," *Cement and Concrete Research*, vol. 34, no. 6, pp. 927–934, 2004. https://doi.org/10.1016/j.cemconres.2003.10.022

[5] A. Martínez‐Molina, I. Tort‐Ausina, S. Cho, and J. L. Vivancos, "Energy efficiency and thermal comfort in historic buildings: A review," *Renewable and Sustainable Energy Reviews*, vol. 61, pp. 70–85, 2016. https://doi.org/10.1016/j.rser.2016.03.018

[6] V. De Giuli, O. Da Pos, and M. De Carli, "Indoor environmental quality and pupil perception in Italian primary schools," *Building and Environment*, vol. 56, pp. 335–345, 2012. https://doi.org/10.1016/j.buildenv.2012.03.024

[7] P. K. Latha, Y. Darshana, and V. Venugopal, "Role of building material in thermal comfort in tropical climates – A review," *Journal of Building Engineering*, vol. 3, pp. 104–113, 2015. https://doi.org/10.1016/j.jobe.2015.06.003

[8] J. Gui et al., "Impact of pavement thermophysical properties on surface temperatures," *Journal of Materials in Civil Engineering*, vol. 19, no. 8, pp. 683–690, 2007. https://doi.org/10.1061/(ASCE)0899-1561(2007)19:8(683)

[9] L. Daza et al., "Thermal conductivity in mortar samples with copper mine tailings," *Materials*, vol. 18, no. 13, p. 3157, 2025. https://doi.org/10.3390/ma18133157

[10] Z. A. Mohammed et al., "Effect of steel fibers and iron filings on concrete properties with partial replacement of cement by fly ash," *Journal of Techniques*, vol. 7, no. 1, pp. 56–65, 2025. https://doi.org/10.51173/jt.v7i1.2638

[11] A. Lyons, *Materials for architects and builders*. Routledge, 2014.

[12] A. M. Neville, *Properties of Concrete*, 4th ed. London, U.K.: Longman, 1995.

[13] M. N. H. Al‑Hashimi et al., "Performance of concrete containing iron fillings," *Journal of University of Babylon for Engineering Sciences*, vol. 26, no. 6, pp. 384–392, 2018.

[14] Y. Sargam et al., "Effects of modern concrete materials on thermal conductivity," *Journal of Materials in Civil Engineering*, vol. 32, no. 4, p. 04020058, 2020. https://doi.org/10.1061/(ASCE)MT.1943-5533.0003026

[15] A. E. Díaz et al., "Experimental study to measure conductive heat transfer properties in new materials with environmental waste aggregates," *American Journal of Physics and Applications*, vol. 13, no. 2, pp. 10–11648, 2025. https://doi.org/10.11648/j.ajpa.20251302.11

[16] G. Li et al., "Experimental investigation of thermal and mechanical characteristics of slag cement mortars with PCM for radiant floors," *Case Studies in Construction Materials*, vol. 20, p. e02958, 2024. https://doi.org/10.11648/j.ajpa.20251302.11

[17] S. T. Jeong et al., "Thermal performance of concrete containing graphite at high temperatures for the application in a TES," *Energies*, vol. 18, no. 17, p. 4685, 2025. https://doi.org/10.3390/en18174685

[18] J. Y. Kim et al., "Site application of thermally conductive concrete pavement: A comparison of its thermal effectiveness with normal concrete pavement," *Materials*, vol. 18, no. 15, p. 3444, 2025. https://doi.org/10.3390/ma18153444

[19] C. Chen et al., "Developing heat conductive concrete with graphite‑modified recycled aggregates," *Composites Part B: Engineering*, vol. 271, p. 111721, 2024. https://doi.org/10.1016/j.compositesb.2024.111721

[20] F. Jafari et al., "Evaluating thermal storage capability of recycled construction materials: An experimental approach," *Materials for Renewable and Sustainable Energy*, vol. 14, no. 25, 2025. https://doi.org/10.1007/s40243-025-00299-6

[21] A. Jabri et al., "Feasibility of the performance of thermal photovoltaic systems in residential units in the climate of four cities of Abadan, Baghdad, Basra, and Tehran in terms of energy saving," *Journal of Applied and Computational Sciences in Mechanics*, vol. 35, no. 3, pp. 33–50, 2023. https://doi.org/10.22067/jacsm.2023.79017.1141

[22] F. V. Inia et al., "Evaluation of energy and exergy of a parabolic trough solar collector equipped with internal fin and star turbulator absorber tube," *Journal of Applied and Computational Sciences in Mechanics*, vol. 36, no. 2, pp. 97–114, 2024. https://doi.org/10.22067/jacsm.2023.83484.1199

[23] M. R. Kalateh et al., "Experimental study and numerical modeling of the effect of utilizing selected twisted tape insert on the performance of thermal photovoltaic system," *Journal of Applied and Computational Sciences in Mechanics*, vol. 33, no. 2, pp. 1–22, 2022. https://doi.org/10.22067/jacsm.2022.74538.1083

[24] A. Arabsolghar et al., "Investigation of down‑draught effect on the thermal comfort indexes in the building with glazing envelope," *Journal of Applied and Computational Sciences in Mechanics*, vol. 33, no. 1, pp. 35–52, 2021. https://doi.org/10.22067/jacsm.2021.70588.1030

[25] A. Amiri et al., "Investigating the effect of phase change materials on energy consumption in lightweight prefabricated relief buildings," *Journal of Applied and Computational Sciences in Mechanics*, vol. 34, no. 4, pp. 35–52, 2022. https://doi.org/10.22067/jacsm.2022.78503.1136

[26] L. S. Fletcher, *Recent developments in contact conductance heat transfer*, 1988. https://doi.org/10.1115/1.3250610

[27] J. F. Mallory,*Thermal Insulation*, *Reinhold* ,New York, pp. 13-17,1969.

[28] D. Taoukil et al., "Moisture content influence on the thermal conductivity and diffusivity of wood–concrete

composite," *Construction and Building Materials*, vol. 48, pp. 104–115, 2013. https://doi.org/10.1016/j.conbuildmat.2013.06.067

[29] D. Taoukil et al., "Moisture content influence on the thermal conductivity and diffusivity of wood–concrete composite," *Construction and Building Materials*, vol. 48, pp. 104–115, 2013. https://doi.org/10.1016/j.conbuildmat.2013.06.067

[30] S. Klarsfeld et al., "Guarded hot plate method for thermal conductivity measurements," *Compendium of Thermophysical Property Measurement Methods*, vol. 1, p. 169, 1984. https://doi.org/10.1007/978-1-4615-6678-6_5

[31] A. S. Gandage et al., "Effect of perlite on thermal conductivity of self-compacting concrete," *Procedia – Social and Behavioral Sciences*, vol. 104, pp. 188–197, 2013. https://doi.org/10.1016/j.sbspro.2013.11.111

[32] U. J. Alengaram et al., "A comparison of the thermal conductivity of oil palm shell foamed concrete with conventional materials," *Materials & Design*, vol. 51, pp. 522–529, 2013. https://doi.org/10.1016/j.matdes.2013.04.078

[33] Equipment M E B T D, Compendium of thermophysical property measurement methods, 1992. https://doi.org/10.1007/978-1-4615-3286-6?nosfx=y

[34] W. N. dos Santos et al., "Numerical and experimental determination of the minimum and maximum measuring times for the hot wire parallel technique," *Cerâmica*, vol. 49, pp. 29–35, 2003. https://doi.org/10.1590/S0366-69132003000100007

[35] M. Bederina et al., "Effect of the addition of wood shavings on thermal conductivity of sand concretes: Experimental study and modelling," *Construction and Building Materials*, vol. 21, no. 3, pp. 662–668, 2007. https://doi.org/10.1016/j.conbuildmat.2005.12.008

[36] H. Q. Jin et al., "Experimental determination and fractal modeling of the effective thermal conductivity of autoclaved aerated concrete: Effects of moisture content," *International Journal of Heat and Mass Transfer*, vol. 92, pp. 589–602, 2016. https://doi.org/10.1016/j.ijheatmasstransfer.2015.08.103

[37] L. Wadsö et al., "Thermal properties of concrete with various aggregates," *Cement and Concrete Research*, vol. 25, 2012.

[38] J. Chan, "Thermal properties of concrete with different Swedish aggregate materials," Rapport TVBM (5000-serie), 2014.

[39] W. H. Rohsenow et al., *Handbook of heat transfer*. New York: Mcgraw-hill, 1998.

[40] B. P. Jelle, "Traditional, state-of-the-art and future thermal building insulation materials and solutions – properties, requirements and possibilities," *Energy and Buildings*, vol. 43, no. 10, pp. 2549–2563, 2011. https://doi.org/10.1016/j.enbuild.2011.05.015

[41] E. Barreira et al., "Evaluation of building materials using infrared thermography," *Construction and Building Materials*, vol. 21, no. 1, pp. 218–224, 2007. https://doi.org/10.1016/j.conbuildmat.2005.06.049

[42] J. R. Cannon, *The One-Dimensional Heat Equation*, no. 23, Cambridge University Press, 1984.

[43] T. L. Bergman, *Fundamentals of heat and mass transfer*. John Wiley & Sons, 2011.

[44] C. Meyer, "The greening of the concrete industry," *Cement and Concrete Composites*, vol. 31, no. 8, pp. 601–605, 2009. https://doi.org/10.1016/j.cemconcomp.2008.12.010

[45] K. Sudalaiyandi et al., "Performance and emission characteristics of diesel engine fueled with ternary blends of linseed and rubber seed oil biodiesel," *Fuel*, vol. 285, p. 119255, 2021. https://doi.org/10.1016/j.fuel.2020.119255

[46] S. J. Kline, "Describing uncertainties in single-sample experiments," *Mechanical Engineering*, vol. 75, pp. 3–8, 1963.

[47] A. M. Neville, *Properties of Concrete*, 5th ed. Pearson Education Limited, 2011.

[48] K. H. Kim et al., "An experimental study on thermal conductivity of concrete," *Cement and Concrete Research*, vol. 33, no. 3, pp. 363–371, 2003. https://doi.org/10.1016/S0008-8846(02)00965-1

[49] X. C. Tong, "Characterization methodologies of thermal management materials," in *Advanced Materials for Thermal Management of Electronic Packaging*, New York, NY: Springer, 2010, pp. 59–129.. https://doi.org/10.1007/978-1-4419-7759-5_2

[50] W. Zhang et al., "Mesoscale model for thermal conductivity of concrete," *Construction and Building Materials*, vol. 98, pp. 8–16, 2015. https://doi.org/10.1016/j.conbuildmat.2015.08.106

[51] I. Budaiwi et al., "Variations of thermal conductivity of insulation materials under different operating temperatures: Impact on envelope-induced cooling load," *Journal of Architectural Engineering*, vol. 8, no. 4, pp. 125–132, 2002. https://doi.org/10.1061/(ASCE)1076-0431(2002)8:4(125)

[52] F. Kanibou et al., "Thermophysical properties of concrete blended with iron powder and/or iron fibers," *Civil and Environmental Engineering*, vol. 20, no. 1, pp. 293–306, 2024. https://doi.org/10.2478/cee-2024-0023